



Use of Reverse Electrodialysis to Harvest Salinity Gradient Energy from Oilfield Produced Water

Talib Abbas*, Mustafa Al-Furaiji

Environment and Water Directorate, Ministry of Science and Technology, Baghdad, Iraq

Received: 23 May 2021, Revised: 09 August 2021, Accepted: 18 September 2021

ABSTRACT

Two lab-scale electro dialysis (RED) stacks with different intermembrane spacing were used in this study. Each stack consists of two membrane pairs. Thick intermembrane spacing stack was made of four identical plexiglass sections, with outer dimensions 5 cm * 5 cm * 1.5 cm and an inner cross-section of 3 cm diameter each to construct two diluted solution compartments and two concentrated solution compartments. For the thin intermembrane spacing configuration, four rubber spacers with a thickness of 1 mm and an inner opening of 3 cm each were used instead of these sections. Two copper sheets were used as anode and cathode electrodes. Different solutions with NaCl concentrations of 15,000, 30,000 and 200,000 mg/l were used as a concentrated solution and different solutions with relatively low NaCl concentrations of 25, 1000 and 3600 mg/l were used as a diluted solution. A 30,000 mg/l NaCl solution was used as a diluted solution when the concentrated stream was with NaCl concentration of 200,000 mg/l. The electrode solution was of 15,000 mg/l (~0.25 M) NaCl and 8,000 mg/l (~0.05 M) $\text{CuSO}_4 \cdot 5\text{H}_2\text{O}$. The results of this study confirmed the validity of using RED technology to harvest energy from salinity gradient using saline and freshwater available abundantly particularly in Iraq. An experiment on a synthetic hypersaline oil field co-produced water as a concentrated stream and seawater as a diluted stream showed that the system performance is reproducible and stable. A maximum power density of 0.029 W/m² could be harvested.

Keywords: Electrode; Ion exchange membrane; Anode; Cathode.

INTRODUCTION

Conventional energy sources usually cause high pollution effects besides their large operating and capital costs (Alalwan et al., 2021; Alalwan and Alminshid, 2021; Alminshid et al., 2021; Hassan et al., 2021). Recently, there has been a growing interest in exploring more possible renewable energy sources. Salinity gradient power (SGP) is a promising way to harvest chemical energy potential when mixing two water streams with different salinities. The concept of SGP was first presented by Pattle (1954). In general, there are two different techniques to recover this potential energy: pressure retarded osmosis (PRO) and reverse electro dialysis (RED). In PRO, the chemical potential (osmotic) energy is converted into mechanical energy (then to electrical energy using turbines) with the aid of forward osmosis membranes (Al-Furaiji et al., 2020). On the other hand, in RED the chemical potential energy is converted directly into electrical energy with the aid of ion-exchange membranes (IEM's) (Tedesco et al., 2012).

In RED systems, a stack of ion exchange membranes (IEM) is used). Tens of parallel successive pairs, with cation exchange membrane (CEM) and anion exchange membrane (AEM) each, are used to form alternative diluted streams and concentrated streams compartments. Spacers might be used to separate adjacent membranes. Positive ions are

* Corresponding author Email: talibrshd@yahoo.com

transported through the CEMs and negative ions are transported in the opposite direction through the AEMs from concentrated streams to dilute streams. Due to this process, an electrical potential is formed across the RED stack which can be converted into DC electrical current flowing into an external electrical circuit connected across the stack through redox reactions at the electrodes (Avci et al., 2018; Bodner et al., 2019; Castaño, 2016; Huang et al., 2018; Tedesco et al., 2015).

Electrodes system plays an important role in the RED operation. This system comprises electrodes with their compartments filled with common suitable electrolytes circulated between them. The electrodes system function is to convert ionic current into electric current through redox reactions. There are two categories of electrodes systems, one of them with opposite electrode reactions while the other is without opposite electrode reactions. The latter involves unwanted gas (H_2 , Cl_2 , O_2) generation associated with voltage loss while the former, which is frequently used, involves opposite reactions in which there is no net chemical reactions and no voltage loss. Examples of opposite electrode reactions electrodes system are (Cu-CuSO₄) system, (Zn-ZnSO₄) system and systems with homogeneous redox couples such as FeCl₃/FeCl₂ (D'Angelo et al., 2017; Veerman et al., 2010).

IME properties and spacers thickness play a governing role in RED system performance. Electrical resistance and permselectivity of the IMEs as well as spacer thickness, and consequently the electrical resistance of solution compartments, are the limiting factors for the output power gained from the RED system (Vermass et al., 2012; Tedesco et al., 2018). Due to the relatively low conductivity of the dilute streams, a thinner spacer in these compartments resulted in lower internal electrical resistance of the RED stack and consequently higher density. Previous studies showed an improvement in power density from 0.56 W/m² to 0.87 W/m² when reducing spacer thickness from 0.5 mm to 0.2 mm. Moreover, another RED system with a power density of 2.2 W/m² when using a spacer thickness of 0.1 mm could be achieved (Mei and Tang, 2018).

Operation with optimum hydrodynamic conditions inside the RED stack can increase its output power density. Fluid velocity in the vicinity of the IEMs interface directly affects the ion transfer inside the stack by reducing diffusion boundary layer thickness (due to turbulence) and consequently concentration polarization effect which resulted in the higher open-circuit voltage of the stack. However, at the same time, increasing the fluid velocity results in higher pressure loss and higher pumping power loss. Increasing the fluid velocity can be achieved by reducing intermembrane distance (thin spacer) taking into consideration a very thin distance may result in fluid channel clogging by foulants present in the feeds, leading to a drastic increase in pressure drop. So, optimum operation conditions should be attended to maximize the net power density (Tufa et al., 2018).

Significant lab-scale contributions have been done in the previous studies to improve RED systems performance while scale-up studies are limited. However, RED stack BV company (Netherlands) was operated the first 5 kW RED pilot plant together with Frisia Zout BV (a European salt company). Moreover, this company in collaboration with many other companies has a plan to build this first real-world RED pilot plant with a capacity of 50kW by mixing seawater and lake freshwater (Tufa et al., 2018).

Up to the author's knowledge, researches concerning the RED system in Iraq are lacking. The aim of this study is to get insight into parameters governing the performance of the RED system and taking into consideration the availability of hypersaline oil-field co-produced water that can be used to harvest energy using RED technology.

MATERIAL AND METHODS

Theoretically, the chemical potential energy harvested by mixing two solutions with different salinity can be given by Gibbs free energy equation:

$$\Delta G_{mix} = 2RT \left[V_D C_D \ln \frac{C_D}{C_M} + V_C C_C \ln \frac{C_C}{C_M} \right] \quad (1)$$

$$C_M = \frac{V_D C_D + V_C C_C}{V_D + V_C} \quad (2)$$

Where G_{mix} is Gibbs free energy of mixing, R is the universal gas constant, T is the temperature in ($^{\circ}$ K), V_D is volume of diluted solution, C_D is molar salinity of the diluted solution, C_M is molar salinity of mixed solution, V_C is the volume of concentrated solution, C_C is molar salinity of the concentrated solution. Applying Eq.(1), when mixing 1 m^3 of seawater and 1 m^3 fresh river water 1.7 MJ energy can be produced. This energy can be increased to 6.1 MJ when 1 m^3 of seawater is mixed with 10 m^3 of fresh river water. Potentially, 23% of the world electricity demand can be harvested by SGP at estuaries where the river's freshwater mixes with salty seawater. Moreover, saline and hypersaline waters such as oil field co-produced water and brine streams from desalination plants can be used for this purpose (Avci et al., 2018; Huang et al., 2018; Tedesco et al., 2012).

The electromotive force generated across a stack of N IEM pairs (the open-circuit voltage, OCV) can be theoretically calculated using the Nernst equation:

$$OCV = \frac{NRT}{F} \left[\frac{\alpha_{CEM}}{z_{ct}} \ln \frac{\gamma_{c,ct} C_c}{\gamma_{d,ct} C_d} + \frac{\alpha_{AEM}}{z_{an}} \ln \frac{\gamma_{c,an} C_c}{\gamma_{d,an} C_d} \right] \quad (3)$$

Where N is the number of IEM pairs, F is Faraday constant, α is the permselectivity of the membrane, z is the valance, γ is the ion activity, C is molar ion concentration, subscripts c , d , ct , and refers to the concentrated solution, diluted solution, cation and anion, respectively. The permselectivity is an important factor to determine OCV. It represents the ability of the IEM to transport cations (excluding anions) in the case of CEM and anions (excluding cations) in the case of AEM. In general, an OCV of 0.16 V can be generated from a pair of ideal (100% permselectivity IEMs) when the concentrated solution is seawater (0.5 M NaCl) and the diluted solution is river water (0.017 M NaCl) are used (Tufa et al., 2018).

Two lab-scale RED system configurations were used in this study. The difference between them is the intermembrane spacing (the width of diluted and concentrated stream compartments).

A RED stack consists of two membrane pairs (Figure 1) was made of plexiglass sections. Four identical sections (Figure 2), with outer dimensions $5 \text{ cm} * 5 \text{ cm} * 1.5 \text{ cm}$ and an inner cross-section of 3 cm diameter each, were used to construct two diluted solution compartments and two concentrated solution compartments. Each section was provided with feeding and withdrawal of working solution openings. Another two cubical sections (Figure 3), each with an outer side length of 5 cm and an inner cross-section of 3 cm diameter, were used as anode and cathode compartments. Anion exchange membranes (AEM) and cation exchange membranes (CEM), (AMI7001S and CMI7000S, Membranes International Inc., respectively) were alternatively placed between the cathode and the anode. Following the supplier's recommendations, all membranes were preconditioned by immersing in 5% NaCl solution for 24 h and rinsed with DI water prior to use, to allow for membrane hydration and expansion.

It should be noted that for the sake of experimental simplicity, the spaces between adjacent membranes were relatively large in comparison with other studies (Kim et al., 2015; Tedesco et

al., 2018). Two copper sheets were cut in a circular shape with about 3 cm diameter and were used as anode and cathode electrodes. The working volume of each compartment was about 10.7 cm^3 , while the working volume of each anode and cathode compartment was about 35 cm^3 . The system was operated in two modes, non-flowing mode and flowing mode. In flowing mode the concentrated and diluted solution was supplied to the stack by gravity from two separate reservoirs. The system was operated at room temperature ($25\text{--}35 \text{ }^\circ\text{C}$). Figure 4 is a photograph of the experimental setup used in this work.

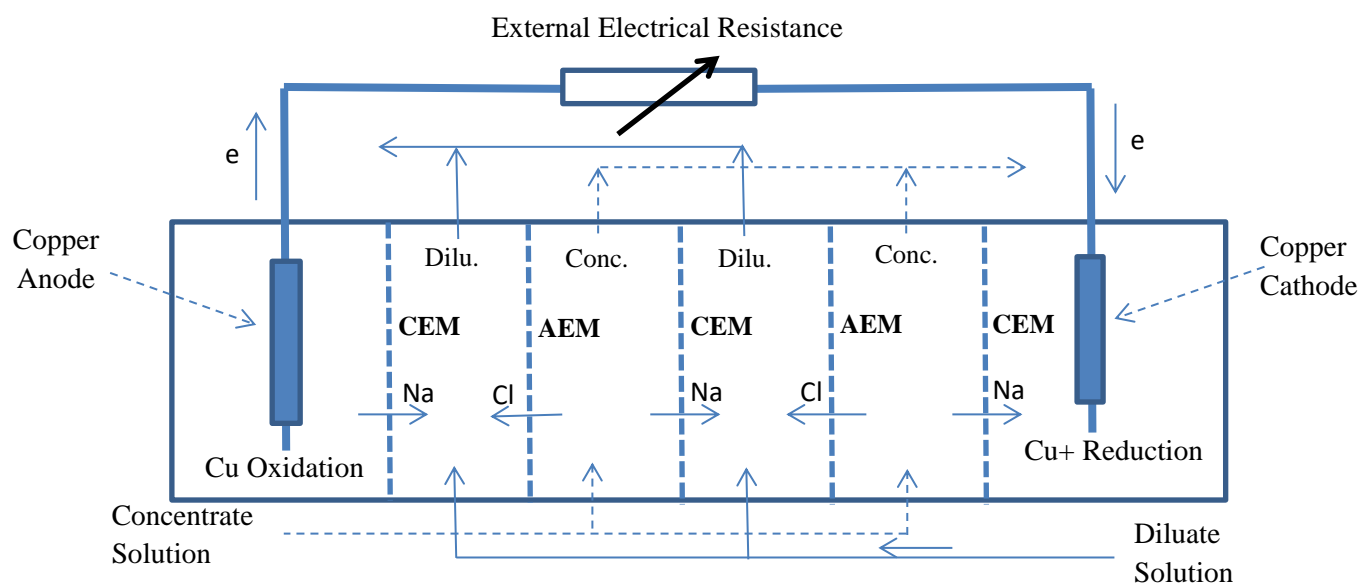


Figure 1. Schematic diagram of the thick intermembrane spacing RED stack.

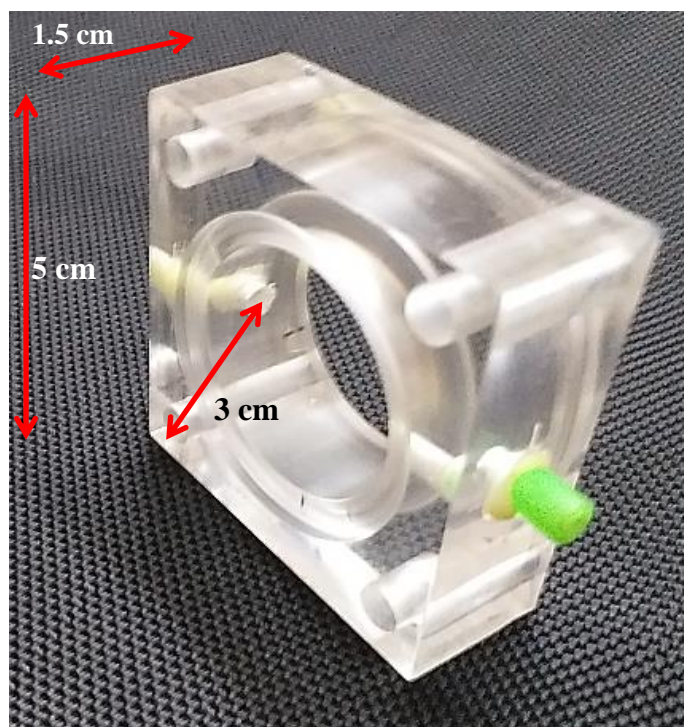


Figure 2. Photograph of one of four sections used to construct concentrated and diluted solutions compartments of the RED stack.

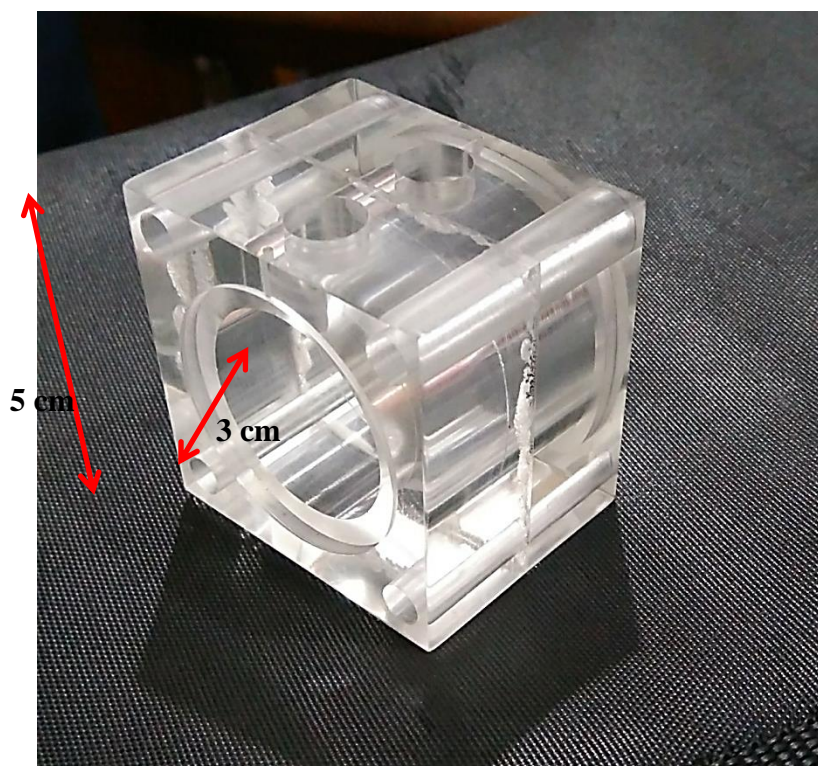


Figure 3. Photograph of one of two cubical sections used to construct anode and cathode compartments of the RED stack.

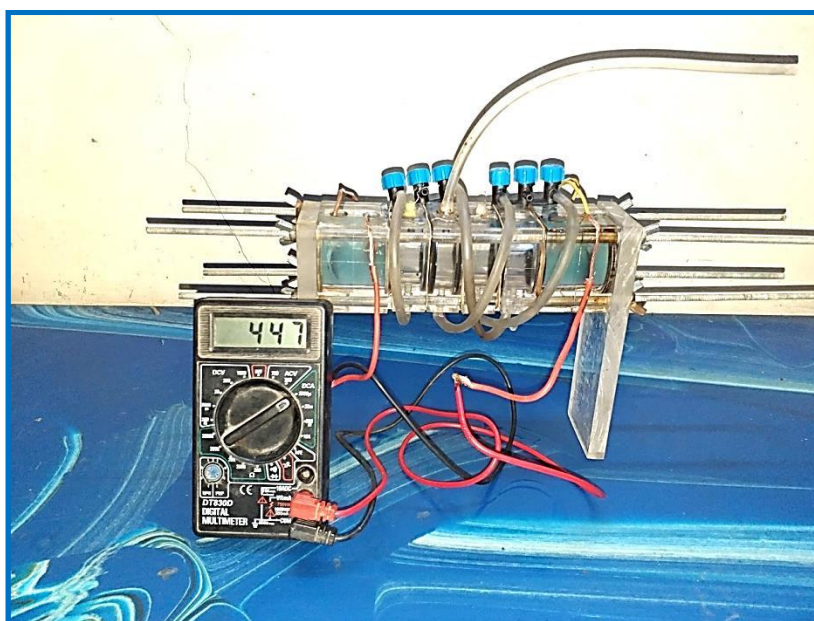


Figure 4. Photograph of the thick intermembrane spacing stack experimental setup.

In this system configuration, four rubber spacers (Figure 5), with a thickness of 1 mm and an inner opening of 3 cm each, were used instead of the four identical plexiglass sections. Similar to the thick intermembrane spacing configuration system described in section 2.1.1, two cubical plexiglass sections (Figure 5), each with an outer side length of 5 cm and inner cross-section of 3 cm diameter, were used as anode and cathode compartments. Copper electrodes were used. Additional plexiglass section with outer dimensions 5 cm * 5 cm * 1.5 cm and inner cross-

section of 3 cm diameter containing two ports as inlet and outlet for a diluted solution and another two ports as inlet and outlet for the concentrated solution of the RED stack. Each rubber spacer was designed to have an inlet flow port at the bottom and an outlet flow port at the top (Coleman Gilstrap, 2013; Hu et al., 2018). When several spacers were aligned in a repeating, inverted fashion, flow routes for the two separate concentrated and diluted solutions are established (Figure 6). The stack was operated in two modes, non-flowing mode and flowing mode. In flowing mode, the concentrated and diluted solutions were supplied to the stack by gravity from two separate reservoirs. The system was operated at room temperature (25–35 °C). Figure 7 is a photograph of the experimental setup used in this work.

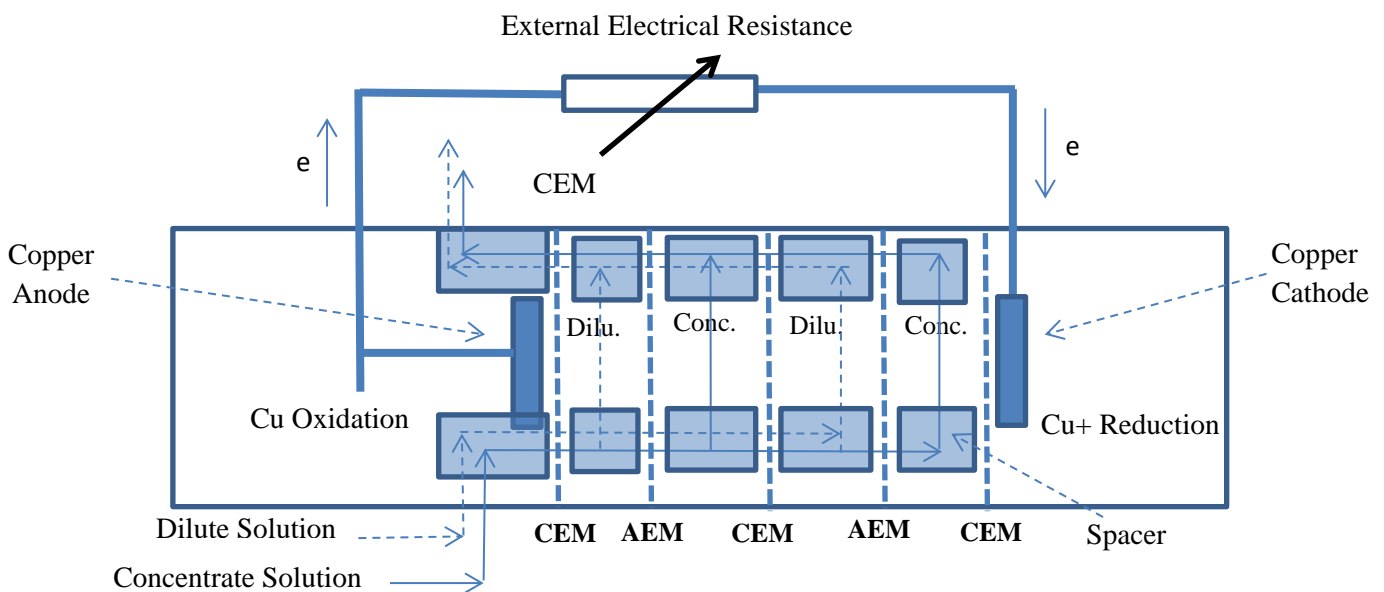


Figure 5. Schematic diagram of the thin intermembrane spacing RED stack.

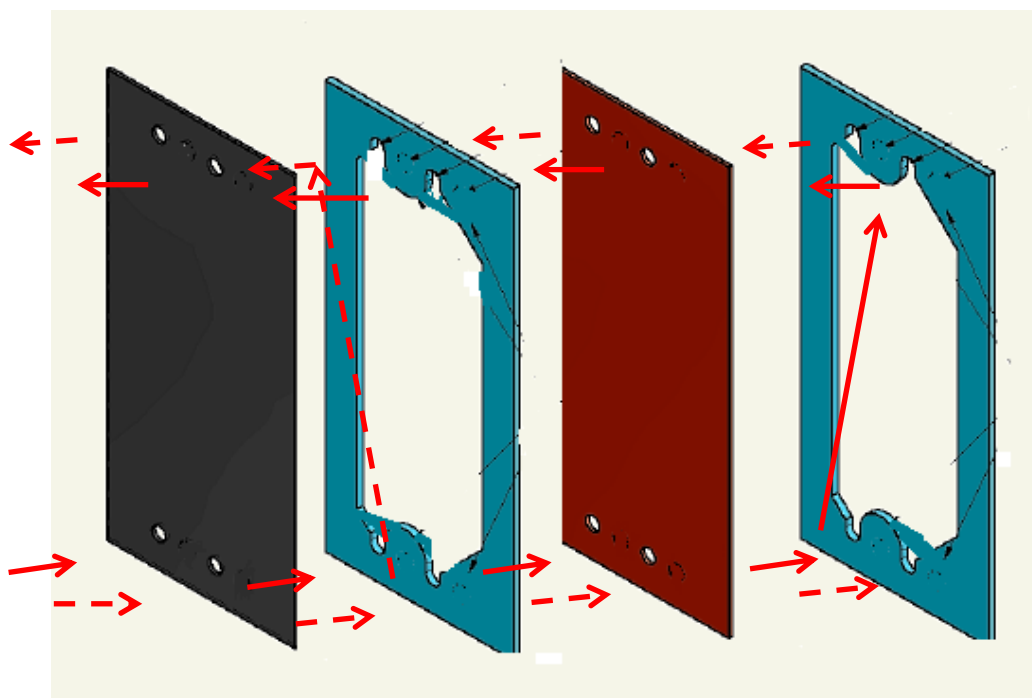


Figure 6. Flow routes driven by spacers in the thin intermembrane spacing RED stack. (the dotted arrow for the concentrated solution and the solid arrow for the diluted solution)

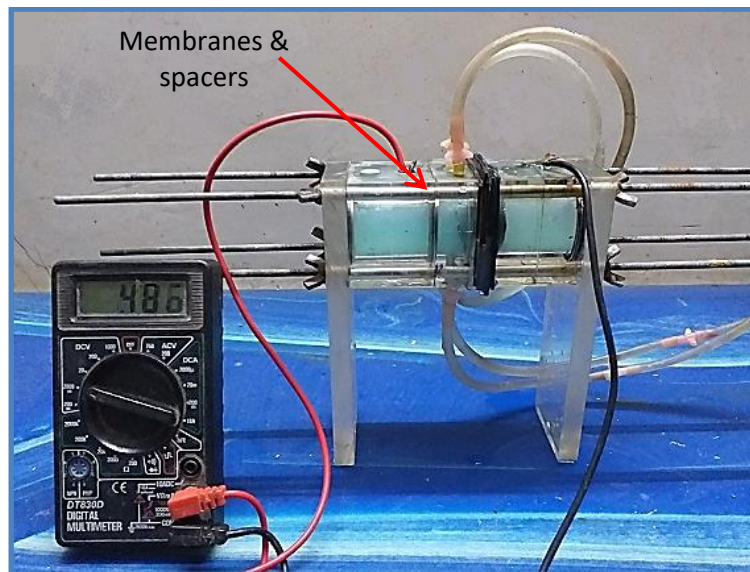


Figure 7. Photograph of the thin intermembrane spacing stack experimental setup.

Different solutions with NaCl concentrations of 15,000, 30,000, and 200,000 mg/l were prepared to be used as a concentrated solution in different experiments. Another set of solutions with relatively low NaCl concentrations of 25, 1000, 3600 and 30,000 mg/l were prepared to be used as the diluted solution. The electrode solution was of 15,000 mg/l (~0.25 M) NaCl and 8,000 mg/l (~0.05 M) $\text{CuSO}_4 \cdot 5\text{H}_2\text{O}$. Synthetic hypersaline water was used to simulate oil field co-produced water in southern part of Iraq with the characteristics presented in Table 1 (Al-Furaiji et al., 2018; Al-rubaie et al., 2015).

Table 1: Characteristics of synthetic oil field co-produced water.

Analysis	Concentration
TDS	250,000 mg/l
Ca^{2+}	15,000 mg/l
Mg^{2+}	3,000 mg/l
Na^+	78,000 mg/l
SO_4^{2-}	100 mg/l
Cl^-	154,000 mg/l

The current (I) flowing through the external resistance (R) and the OCV across the RED stack were measured using a digital multimeter. Electrical conductivity was measured using (Cond 3310, WTW) conductivity meter.

The current density and power density were calculated as follows (Kim et al., 2015):

$$\text{Current density} = \frac{I}{\text{Total Effective Area of AEMs in the Stack}} \quad (4)$$

$$\text{Power density} = \frac{I^2 * R}{\text{Total Effective Area of AEMs in the Stack}} \quad (5)$$

RESULTS AND DISCUSSION

In this experiment, a RED cell with two compartments separated by a CEM was used (Figure 8). Each compartment contains a circular graphite electrode with a diameter of 3 cm. One of the compartments was filled with salty water with TDS of 30,000 mg/l (NaCl) while the other compartments were filled with water with TDS of 25 mg/l. Figure 9 shows the variation of OCV with time. It was clear from this figure that the OCV has a maximum value of 137 mV at the beginning of the experiment. With the aid of Equation 3, the value of the permselectivity of the CEM used in this study was about 0.75. The value of OCV decreased with time due to the co-transport of cations and anions from the high salinity compartment to the low salinity compartment causing the electric conductivity in the low salinity compartment to increase with time as shown in Figure 10. The electrical conductivity in this compartment was increased from 33.8 $\mu\text{S}/\text{cm}$ at the beginning of the experiment to about 140 and 180 $\mu\text{S}/\text{cm}$ after 3 and 6 hr, respectively. The OCV has reached about 114.5 mV after 6 hr from the beginning of the experiment.



Figure 8. Photograph of the two compartments RED cell.

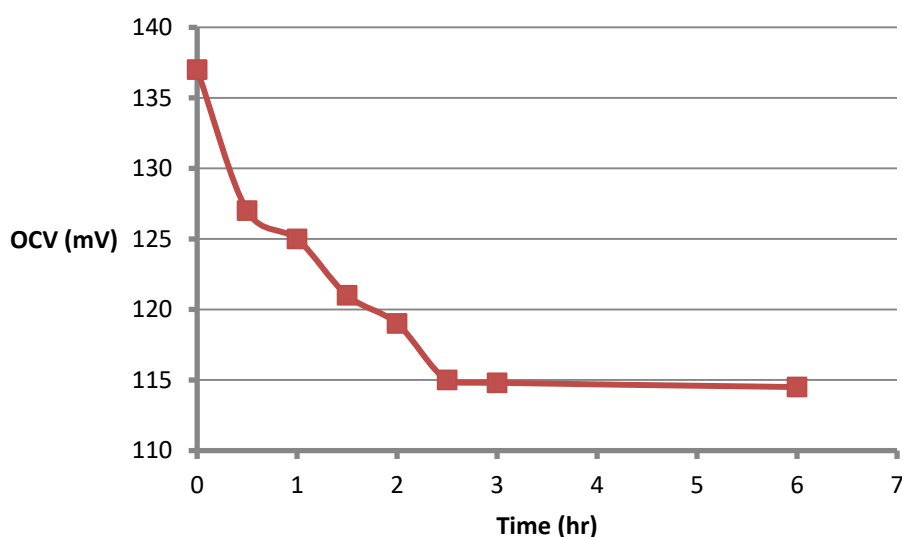


Figure 9. Variation of OCV with time for two compartments RED cell with CEM.

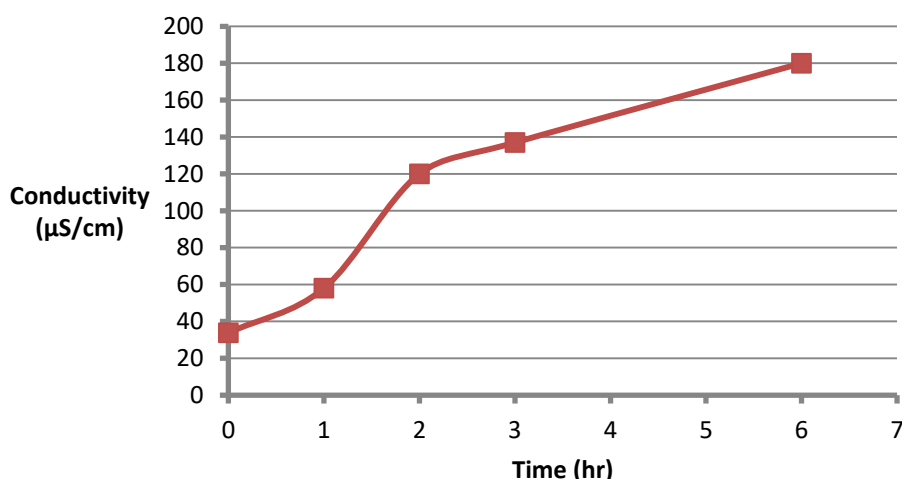


Figure 10. Variation of electrical conductivity of the diluted water with time for the two compartments RED cell with CEM.

In this experiment, an AEM was separated from the concentrated water and diluted water compartments of the two compartments RED cell. The resulting OCV was with reverse polarity relative to the CEM experiment. The OCV at the beginning of the experiment was about 154 mV as shown in Figure 11. OCV, in this case, is higher than that in the case of CEM which reflects a higher permselectivity for AEM than for CEM. Using Equation 3 the value of the permselectivity of the AEM used in this study was about 0.84. However, higher rate of reduction in OCV in this case than that in the case of AEM. The OCV reaches about 99 mV after 6 hr from the beginning of the experiment. This can be attributed to a higher diffusion constant of co-ions through AEM than in CEM. Consequently, higher increase rate of electrical conductivity in the diluted compartment (Figure 12) than in the case of CEM. It reached 224 $\mu\text{S}/\text{cm}$ after 6 hr.

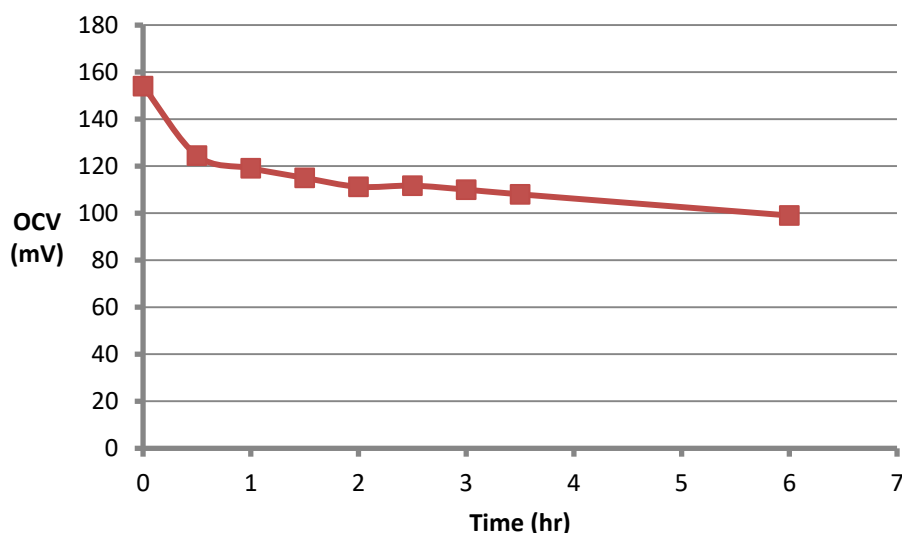


Figure 11. Variation of OCV with time for the two compartments RED cell with AEM.

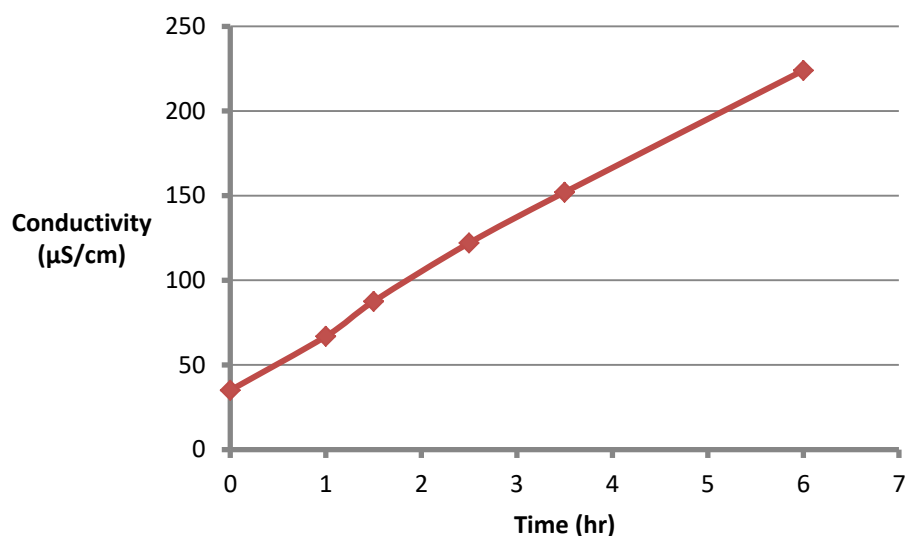


Figure 12. Variation of electrical conductivity of the diluted water with time for the two compartments RED cell with AEM.

Figure 13 shows the effect of salt concentration of diluted water used in the RED stack with thick intermembrane spacing when the salt concentration of concentrated water was 30,000 mg/l. It is clear that the value of OCV is decreased with the increase of diluted compartments salt concentration, starting from about 468 mV at very low salt concentration down to 248 and 163 mV at 1000 and 3600 mg/l, respectively. This can be attributed to the decrease in salinity gradient and can be predicted by Equation 3.

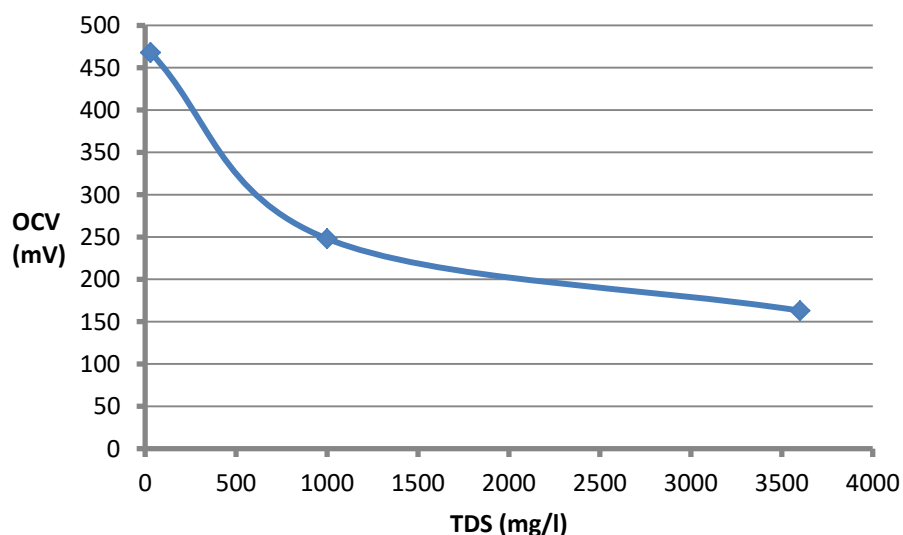


Figure 13. Variation of OCV with salt concentration of diluted water, thick intermembrane spacing, concentrated water TDS = 30,000 mg/l.

Using variable external electrical resistance connected between the anode and the cathode the power density (power per unit area of total AEM in the RED stack) curve was constructed when the salinity of the concentrated water was 30,000 mg/l with different salt concentrations of diluted water as shown in Figure 14. This Figure shows that a maximum power density of about 0.025 W/m^2 could be obtained from the system when the diluted water salt concentration

was 1,000 mg/l which was higher than 0.002 W/m^2 that for dilute water salt concentration of 25 mg/l due to the higher electrical conductivity of water in diluted compartments and higher than 0.018 W/m^2 the case when the diluted water salt concentration was 3600 mg/l due to higher salinity gradient across CEM's and AEM's. In general, the values of the power density obtained in this configuration is lower than those presented in other studies (Kim et al., 2015; Loza et al., 2020; Tufa et al., 2018; Vermaas et al., 2012) which can be attributed to the relatively large intermembrane spacing resulting in relatively high internal electrical resistance preventing the RED stack to produce higher electrical current and consequently higher power density.

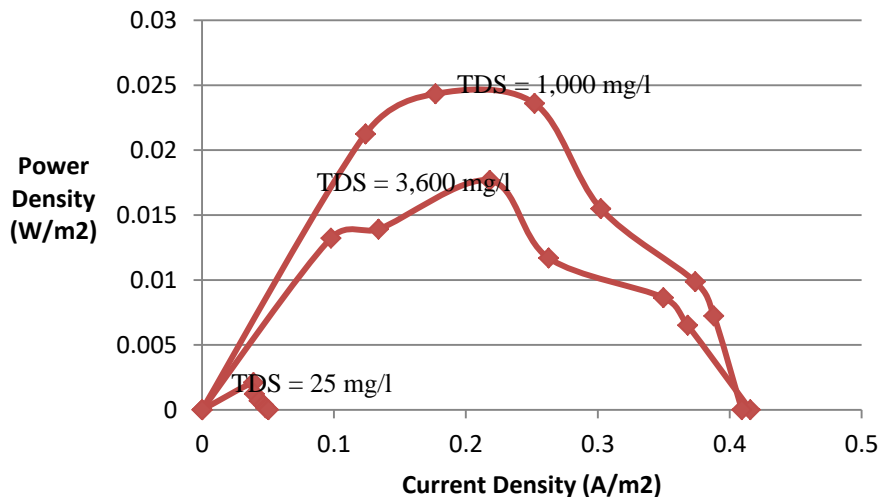


Figure 14. Power density vs. current density for different diluted water TDS, thick intermembrane spacing, concentrated water TDS = 30,000 mg/l.

The effect of concentrated and diluted water flow velocity on the generated power density by RED stack is shown in Figure 15. An increase of flow rate from 0.246 to 0.29 l/min resulted in maximum power density being increased from 0.027 to 0.041 W/m^2 . This can be attributed to the reduction in thickness of boundary layer and hence reduction in concentration polarization effect. However, the increase in pumping energy due to an increase in flow rate should be considered.

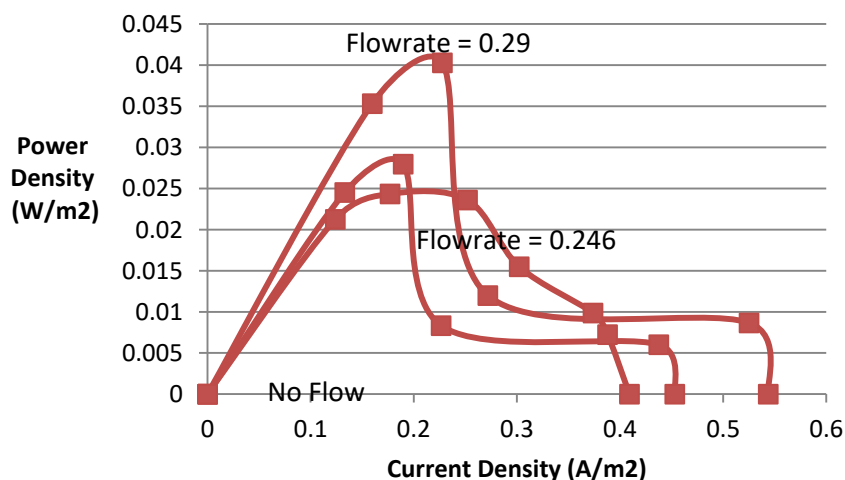


Figure 15. Power density vs. current density for different water flowrate, thick intermembrane spacing, concentrated water TDS = 30,000 mg/l, diluted water TDS = 1,000 mg/l.

To simulate the RED stack behavior when using hypersaline as a concentrated water brine with TDS of 200,000 mg/l was used as concentrated water. The diluted water was with TDS of 1000 mg/l (river water) and 30,000 mg/l (seawater). Higher power density is obtained in the case of freshwater due to the higher salinity gradient. The maximum power density was 0.051 and 0.01 W/m² for 1000 mg/l and 30,000 mg/l, respectively, as shown in Figure 16.

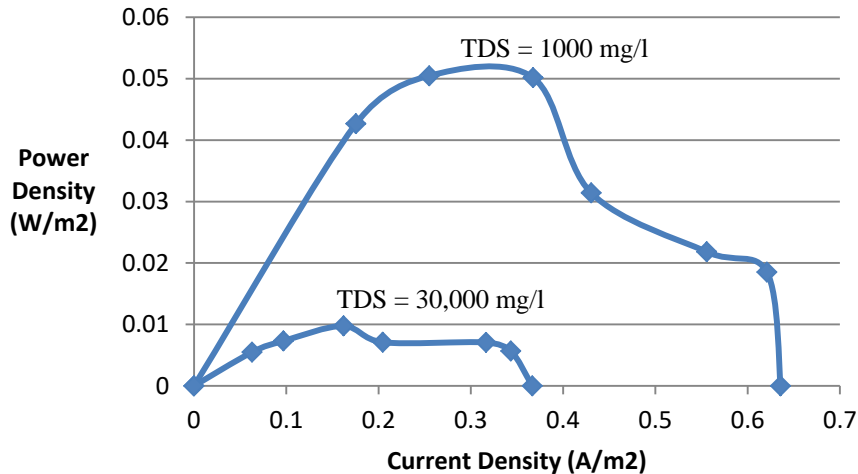


Figure 16. Power density vs. current density for different diluted water TDS, thick intermembrane spacing, concentrated water TDS = 200,000 mg/l.

The RED stack configuration described in suction 3.1.2 was used to assess the effect of intermembrane spacing on the stack performance. Figure 17 shows the power density curve when using concentrated water TDS of 30,000 mg/l and diluted water TDS of 1,000 mg/l. The maximum power density achieved by this configuration was 0.062 and 0.059 W/m² when the flow rate of the two streams was 0.06 and 0 L/min, respectively. In comparison with the RED stack with thick intermembrane spacing in which the maximum power density achieved was 0.041 W/m² it is clear that reduction in intermembrane spacing resulted in an increase in power density. More experimental work with more reduction in intermembrane spacing is needed to obtain the optimum RED stack configuration.

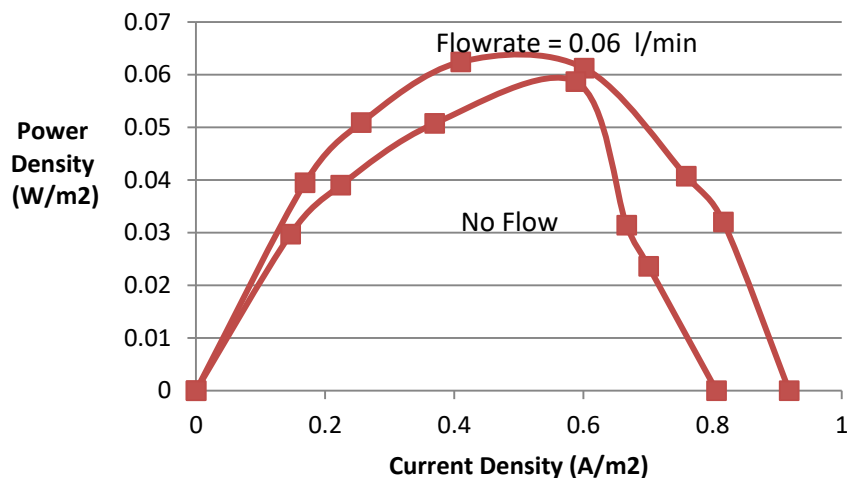


Figure 17. Power density vs. current density, thin intermembrane spacing, concentrated water TDS = 30,000 mg/l, diluted water TDS = 1,000 mg/l.

In this experiment, the synthetic oil field co-produced water with the characteristics presented in Table 1 was used as concentrated water. The diluted water was with TDS of 30,000 mg/l to simulate seawater. The performance of the RED stack with thin intermembrane spacing is shown in Figure 18. A maximum power density of 0.029 W/m^2 can be achieved by this system. The performance of this system is reproducible and stable. However, more experimental work is needed on actual oil field co-produced water after pretreatment. The effect of a relatively high concentration of divalent ions needs to be investigated.

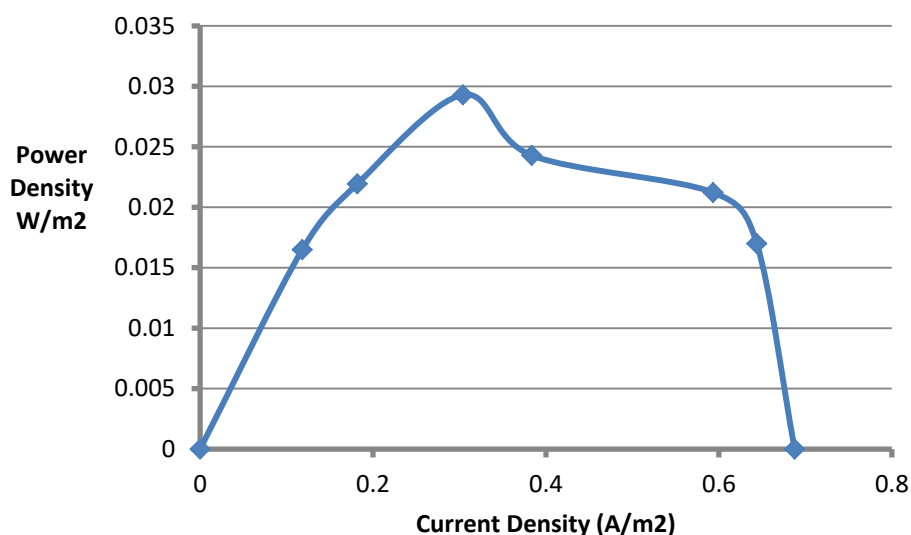


Figure 18. Water TDS = 250,000 mg/l, diluted water TDS = 30,000 mg/l, flowrate = 0.06 l/min.

CONCLUSION

The results of this study confirmed the conceptual validity of using RED technology to harvest energy from salinity gradient using saline and freshwater available abundantly in Iraq. Intermembrane spacing and diluted and concentrated water flow rate are the main governing factors of the system performance. Less intermembrane spacing and higher water flow rate result in higher power density. More experimental work with more reduction in intermembrane spacing and different types of electrode systems is needed to obtain the optimum RED stack configuration. Experiments on a synthetic hypersaline oil field co-produced water as a concentrated stream and seawater as a diluted stream showed that the system performance is reproducible and stable. However, more experimental work is needed on actual Iraqi oil field co-produced water after pretreatment. The effect of a relatively high concentration of divalent ions needs to be investigated.

GRANT SUPPORT DETAILS

The present research did not receive any financial support.

CONFLICT OF INTEREST

The authors declare that there is not any conflict of interests regarding the publication of this manuscript. In addition, the ethical issues, including plagiarism, informed consent, misconduct, data fabrication and/ or falsification, double publication and/ or submission, and redundancy has been completely observed by the authors.

LIFE SCIENCE REPORTING

No life science threat was practiced in this research.

REFERENCES

- Al-Furaiji, M., Kadhom, M., Kalash, K., Waisi, B. and Albayati, N. (2020). Preparation of thin-film composite membranes supported with electrospun nanofibers for desalination by forward osmosis. *Drink. Water Eng. Sci.* 13, 51–57. <https://doi.org/10.5194/dwes-13-51-2020>
- Al-Furaiji, M.H.O., Arena, J.T., Chowdhury, M., Benes, N., Nijmeijer, A. and McCutcheon, J.R. (2018). Use of forward osmosis in treatment of hyper-saline water. *Desalin. Water Treat.* 133, 1–9. <https://doi.org/10.5004/dwt.2018.22851>
- Al-Rubaie, M.S., Dixon, M.A. and Abbas, T.R. (2015). Use of flocculated magnetic separation technology to treat Iraqi oilfield co-produced water for injection purpose. *Desalin. Water Treat.* 53, 2086–2091. <https://doi.org/10.1080/19443994.2013.860400>
- Alalwan, H.A. and Alminshid, A.H. (2021). CO₂ capturing methods: Chemical looping combustion (CLC) as a promising technique. *Sci. Total Environ.* 788, 147850. <https://doi.org/10.1016/j.scitotenv.2021.147850>
- Alalwan, H.A., Augustine, L.J., Hudson, B.G., Abeyasinghe, J.P., Gillan, E.G., Mason, S.E., Grassian, V.H. and Cwiertny, D.M. (2021). Linking Solid-State Reduction Mechanisms to Size-Dependent Reactivity of Metal Oxide Oxygen Carriers for Chemical Looping Combustion. *ACS Appl. Energy Mater.* 4, 1163–1172. <https://doi.org/10.1021/acsaem.0c02029>
- Alminshid, A.H., Abbas, M.N., Alalwan, H.A., Sultan, A.J. and Kadhom, M.A. (2021). Aldol condensation reaction of acetone on MgO nanoparticles surface: An in-situ drift investigation. *Mol. Catal.* 501, 111333. <https://doi.org/10.1016/j.mcat.2020.111333>
- Avci, A.H., Tufa, R.A., Fontananova, E., Di Profio, G. and Curcio, E. (2018). Reverse Electrodialysis for energy production from natural river water and seawater. *Energy* 165, 512–521. <https://doi.org/10.1016/j.energy.2018.09.111>
- Bodner, E.J., Saakes, M., Sleutels, T., Buisman, C.J.N. and Hamelers, H.V.M. (2019). The RED Fouling Monitor: A novel tool for fouling analysis. *J. Memb. Sci.* 570–571, 294–302. <https://doi.org/10.1016/j.memsci.2018.10.059>
- Castañó, S.V. (2016). Energy generation from salinity gradients through Reverse Electrodialysis and Capacitive Reverse Electrodialysis Energy generation from salinity gradients through Reverse Electrodialysis and Capacitive Reverse Electrodialysis 103.
- Coleman Gilstrap, M. (2013). Renewable electricity generation from salinity gradients using reverse electrodialysis.
- D'Angelo, A., Tedesco, M., Cipollina, A., Galia, A., Micale, G. and Scialdone, O. (2017). Reverse electrodialysis performed at pilot plant scale: Evaluation of redox processes and simultaneous generation of electric energy and treatment of wastewater. *Water Res.* 125, 123–131. <https://doi.org/10.1016/j.watres.2017.08.008>
- Hassan, Q.H., Shaker Abdul Ridha, G., Hafedh, K.A.H. and Alalwan, H.A. (2021). The impact of Methanol-Diesel compound on the performance of a Four-Stroke CI engine. *Mater. Today Proc.* 42, 1993–1999. <https://doi.org/10.1016/j.matpr.2020.12.247>
- Hu, J., Xu, S., Wu, X., Wu, D., Jin, D., Wang, P. and Leng, Q. (2018). Theoretical simulation and evaluation for the performance of the hybrid multi-effect distillation—reverse electrodialysis power generation system. *Desalination* 443, 172–183. <https://doi.org/10.1016/j.desal.2018.06.001>
- Huang, Y., Mei, Y., Xiong, S., Tan, S.C., Tang, C.Y. and Hui, S.Y. (2018). Reverse Electrodialysis Energy Harvesting System Using High-Gain Step-Up DC/DC Converter. *IEEE Trans. Sustain. Energy* 9, 1578–1587. <https://doi.org/10.1109/TSTE.2018.2797320>
- Kim, H.-K., Lee, M.-S., Lee, S.-Y., Choi, Y.-W., Jeong, N.-J. and Kim, C.-S. (2015). High power density of reverse electrodialysis with pore-filling ion exchange membranes and a high-open-area spacer. *J. Mater. Chem. A* 3, 16302–16306. <https://doi.org/10.1039/C5TA03571F>

- Loza, S.A., Korzhov, A.N., Loza, N. V. and Romanyuk, N.A. (2020). Energy generation by reverse electro dialysis. IOP Conf. Ser. Mater. Sci. Eng. 791, 012057. <https://doi.org/10.1088/1757-899X/791/1/012057>
- Mei, Y. and Tang, C.Y. (2018). Recent developments and future perspectives of reverse electro dialysis technology: A review. Desalination 425, 156–174. <https://doi.org/10.1016/j.desal.2017.10.021>
- Tedesco, M., Cipollina, A., Tamburini, A., van Baak, W. and Micale, G. (2012). Modelling the Reverse ElectroDialysis process with seawater and concentrated brines. Desalin. Water Treat. 49, 404–424. <https://doi.org/10.1080/19443994.2012.699355>
- Tedesco, M., Hamelers, H.V.M. and Biesheuvel, P.M. (2018). Nernst-Planck transport theory for (reverse) electro dialysis: III. Optimal membrane thickness for enhanced process performance. J. Memb. Sci. 565, 480–487. <https://doi.org/10.1016/j.memsci.2018.07.090>
- Tedesco, M., Mazzola, P., Tamburini, A., Micale, G., Bogle, I.D.L., Papapetrou, M. and Cipollina, A. (2015). Analysis and simulation of scale-up potentials in reverse electro dialysis. Desalin. Water Treat. 55, 3391–3403. <https://doi.org/10.1080/19443994.2014.947781>
- Tufa, R.A., Pawlowski, S., Veerman, J., Bouzek, K., Fontananova, E., di Profio, G., Velizarov, S., Goulão Crespo, J., Nijmeijer, K. and Curcio, E. (2018). Progress and prospects in reverse electro dialysis for salinity gradient energy conversion and storage. Appl. Energy 225, 290–331. <https://doi.org/10.1016/j.apenergy.2018.04.111>
- Veerman, J., Saakes, M., Metz, S.J. and Harmsen, G.J. (2010). Reverse electro dialysis: evaluation of suitable electrode systems. J. Appl. Electrochem. 40, 1461–1474. <https://doi.org/10.1007/s10800-010-0124-8>
- Vermaas, D.A., Guler, E., Saakes, M. and Nijmeijer, K. (2012). Theoretical power density from salinity gradients using reverse electro dialysis. Energy Procedia 20, 170–184. <https://doi.org/10.1016/j.egypro.2012.03.018>